



Water Migration in One-Side Heated Concrete: 4D In-Situ CT Monitoring of the Moisture-Clog-Effect

Bartosz Powierza¹ · Ludwig Stelzner¹ · Tyler Oesch¹ · Christian Gollwitzer¹ · Frank Weise¹ · Giovanni Bruno¹

Received: 22 December 2017 / Accepted: 5 December 2018 / Published online: 18 December 2018
© Springer Science+Business Media, LLC, part of Springer Nature 2018

Abstract

Explosive spalling due to fire exposure in concrete structures can lead severe damage and, in the worst case, to premature component failure. For this reason, an in situ investigation of water migration in concrete due to surface heating was undertaken. During these experiments, a miniaturized concrete specimen within a confining and insulating double-hull was subjected to surface heating during simultaneous X-ray computed tomography (CT) scanning. Through the use of subtraction-based image analysis techniques, it was possible to observe and quantify not only drying within areas of the concrete matrix close to the heated surface, but also the migration of moisture to both pore and matrix regions deeper within the specimen. It was also discovered that the correction of CT images for specimen deformation using DVC and variable detector performance using calibrated image filters significantly improved the quality of the results. This clearly demonstrates the potential of X-ray CT for evaluation of other rapid-density-change phenomena in concrete and other building materials.

Keywords In-Situ · X-ray CT · DVC · Heated concrete · Water migration · Fire

1 Introduction

1.1 Fire in Concrete Structures

Explosive spalling due to fire exposure in concrete structures can lead to severe damage and, in the worst case, to premature component failure. One of the many examples of this phenomenon is the Channel Tunnel fire (November 1996), in which the tunnel lining spalled with a maximum depth of 45 cm and the surrounding rock was exposed [1]. During unilateral thermal exposure, moisture in the portion of a concrete component closest to the fire evaporates and migrates to cooler areas further from the heating source, where it recondenses. This moisture-transport process is constricted by both the low permeability of high-strength concrete (HSC) and the formation of a saturated zone within building components (also known as a moisture clog). This leads to a build-up of water-vapour pressures and contributes to explosive spalling.

This pressure build-up has been verified using pore-pressure measurement techniques [2] and the redistribution of moisture within unilaterally-heated concrete specimens has been demonstrated on fractured surfaces [3]. Investigations by means of the nuclear magnetic resonance (NMR) relaxometry technique [4] and neutron radiography [5, 6] have also shown one-dimensional (1D) changes in moisture distribution during thermal exposure. Results of the first-known three-dimensional (3D) analysis of the moisture transport within unilaterally-heated concrete specimens using X-ray CT have been shown in [7, 8]. However, a quantification of the moisture change during the thermal exposure was not included in that publication. The quantification of the moisture change represents a key parameter for the detailed analysis of the thermally-induced moisture transport. Such a quantitative analysis is presented in this paper, so that conclusions about the changing moisture conditions within the pore structure can be drawn. This is necessary to obtain a better understanding of the underlying damage processes and mechanisms and facilitates the assessment of spalling behaviour in different concretes. Additionally, the quantified moisture distribution can be used as validation data for simulations on the mesoscale.

In principle, neutron CT can provide a 3D picture of the water content distribution in the sample [9]. However,

✉ Bartosz Powierza
bartosz.powierza@bam.de

¹ Bundesanstalt für Materialforschung und -prüfung, Unter den Eichen 87, 12205 Berlin, Germany

access to neutron facilities is very limited and the relatively low brightness of most neutron sources and, consequently, long scanning times, restrict this method to static specimens and limited numbers of samples only [10]. Thus, an analysis method for the measurement of fire-related moisture transport in concrete based on widely available laboratory X-ray CT would be very useful.

1.2 X-ray CT in Concrete Research

X-ray CT has been used in non-destructive concrete research applications for more than 30 years [11, 12]. In this scanning method, a specimen is placed on a rotating table between an X-ray source and an X-ray detector [13]. This causes an X-ray attenuation image of the specimen to be projected upon the detector. By recording these projected images during the 360° rotation of the specimen, the projections can be inverted using volume reconstruction algorithms, which produce a 3D representation of X-ray attenuation within the specimen [14]. The X-ray attenuation, which is dependent on the density of individual component materials within the specimen, can then be identified and objects made from these component materials can be individually separated and analysed.

Previous research has shown that X-ray CT scans can be taken during incremental testing, which may involve both mechanical [15–19] and chemical [20–22] processes, including the transport of water [23–25]. However, the measurement of moisture changes within concrete during thermal exposure presents two particular challenges for in situ X-ray CT. First, image acquisition must be relatively rapid to capture the phenomena, which limits the number and duration of X-ray projections and leads to considerable noise within the images. Second, the moisture changes within the concrete material are relatively small compared to many other water transport processes and the moisture must be measured without the benefit of tracking agents. At the present time, very little work has been reported on fire-related damage processes in concrete using X-ray CT [26].

1.3 Scope

In this work, the thermal-induced moisture transport in concrete was investigated by heating one end of a cylindrical concrete specimen to a temperature of 300 °C and maintaining that temperature 130 min in order to simulate uni-lateral heating. Throughout this process, the density changes in the specimen were measured by means of X-ray CT. After correcting the images for volume-change effects by means of digital volume correlation (DVC), quantitative information about the water transport in the specimen was extracted from difference images obtained by comparing the CT images of the initial, unheated state with subsequent CT images of the heated specimen.

In the next section, the experimental setup of the CT measurement with simultaneous in situ thermal loading is described. This is followed by a detailed description of the image-processing techniques that were used to extract qualitative and quantitative data about the water-transport process. Finally, a discussion of the results of this testing program is presented and conclusions are drawn about how this research affects the current understanding of moisture-transport processes in concrete and the promise of this methodology for future materials research.

2 Experimental Investigation

2.1 Specimens

This investigation focused on the analysis of the moisture transport in unilateral-heated planar building components. Of course, it would, theoretically, be optimal to carry out fire testing and CT scanning on full-scale structural components. However, such full-scale experiments would encounter three significant difficulties, which preclude the practical implementation of such tests. First, 3D imaging of such full-scale components would require the use of specialized, high-power scanning equipment such as a linear accelerator (LINAC). At the high energy levels of such X-ray sources, X-ray scattering effects are expected to play a much larger role than in low-energy scanning, and, thus, to lead to significant degradations in image quality. Second, since there is typically a reduced rate of photon-capture for high-energy scanning of large components, the required scanning times would be significantly increased and it would probably be difficult to acquire sufficient greyscale colour-depth resolution to accurately measure small changes in moisture conditions. Third, most structural-scale elements that are vulnerable to fire-spalling have large dimensional aspect ratios. This means that to obtain 3D images of such objects, the use of laminography techniques rather than tomography would be necessary. This would lead to a further degradation in image quality since projection images from only a limited number of angles are available for laminography reconstructions.

Thus, the chosen measurement technique (X-ray CT) and the necessary temporal and spatial resolution required a suitable specimen size. The short scanning times necessary to adequately observe the moisture-transport phenomenon meant that for thick concrete specimens, which must often possess a diameter exceeding approximately 75 mm in order to provide a representative volume element (RVE), sufficient X-ray illumination of the detector could not be recorded within the permissible image acquisition period. Given the desire to observe moisture transport in small air pores within the material and the fixed pixel-resolution of the detector

Table 1 Mixture of the high-strength concrete

Component	Content (kg/m ³)
Cement (CEM I 42.5 R)	580
Water	173
Aggregate (quarzitic)	
0/2 (mm)	764
2/4 (mm)	229
4/8 (mm)	535
Silica fume	63.8
Superplasticizer	14.5

system, the overall diameter of the specimens had to also be limited.

Within the above-mentioned specimens, the thermal, mechanical and hydraulic boundary conditions had to be controlled in order to mimic a unilaterally-heated planar building component. This led to a specimen with a double-layer casing. The core of the specimen was a slightly conical shaped cylinder made of high-strength concrete. The concrete composition is described in detail in [8] and summarized in Table 1. After casting, the specimens were covered with plastic wrap for one day. Subsequently, the specimens were stored under water until the 28th day following casting. The heating procedure with simultaneous X-ray CT measurements was carried out on specimens that were at least 90 days old, as recommended in [27]. In the period between the storage under water and the heating, the specimens were stored in a climate chamber with a temperature of 20 °C and 65% relative humidity.

To ensure a 1D moisture flux inside the concrete cylinder, the high-strength concrete specimen was surrounded by a glass–ceramic shell made of MACOR. This glass–ceramic was impermeable to water vapour and was intended to prevent radial moisture loss. In addition, the radial thermal expansion of the concrete was hindered by the ceramic shell because of its lower thermal expansion coefficient and high tensile strength, in comparison with the concrete. To achieve a 1D heat flux inside the specimen, the glass–ceramic shell was surrounded by an additional shell made of high-temperature aluminium silicate wool. The heated high-strength concrete surface had a diameter of 4 cm and the total length of the specimen was 10 cm. The overall construction of the specimen with double-layer casing is shown in Fig. 1.

2.2 X-ray CT Setup

Throughout the experiments, a General Electric vltomelx L300 micro-CT system was used to collect X-ray projections. This system contained an X-ray source with a maximum

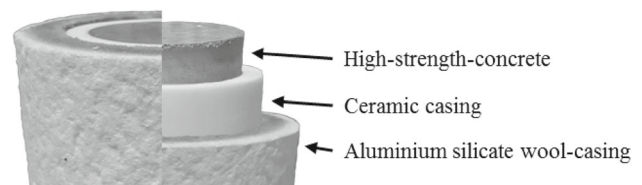


Fig. 1 Construction of the high-strength concrete specimen with ceramic casing and insulation shell made of high-temperature wool

acceleration voltage of 300 kV and a 400 × 400 mm 14-bit detector with 2023 × 2023 pixels. During thermal testing, the source–detector distance was set to 800 mm and the source–specimen (rotation axis) distance to 160 mm. During each scan, 650 projections were collected with an acquisition time of one second per projection. This resulted in a measurement time of 10 min for a full CT scan and a spatial resolution of 160 μm after 4 × 4-binning.

One of the main technical challenges of this experiment was to choose the optimal measurement parameters needed to obtain the best-possible quality of the resulting CT-images. At the same time, a compromise had to be reached between the spatial resolution necessary to visualize the material structure with sufficient accuracy and the temporal and density resolution necessary to observe the rapid density changes. The crucial limitations were, therefore, the requirement that complete scanning times not exceed 15 min each as well as the requirement that specimen diameter not be significantly reduced below 4 cm, which would inhibit the ability of the sample to simulate the heat- and moisture-propagation conditions within a large-scale building component.

In order to determine the optimal X-ray source and pre-filter settings, a number of preliminary test measurements with variable acceleration voltages between 100 and 300 kV and various pre-filters were evaluated (Fig. 2). The settings that produced the image with the highest signal-to-noise ratio were chosen for all subsequent experiments. These settings corresponded to an acceleration voltage of 250 kV, a 0.5 mm copper pre-filter, and an X-ray current of 150 μA (Fig. 2d). Even if at these settings the contrast between the aggregates and the cement matrix is low, these measurement conditions were considered to best facilitate the observation of changes in the moisture content, which is the focus of this study.

2.3 In-Situ Thermal Loading

Figure 3 displays the in situ thermal loading device that was used to generate the surface heating throughout these experiments. The heating was realized by an electrical heating element, which was connected to an electronic controlling unit TR800 Sonder from Bach RC including a Jumo Dicon Touch programme controller. The heating element was an ohmic resistor made of ceramic (silicon nitride). It was posi-

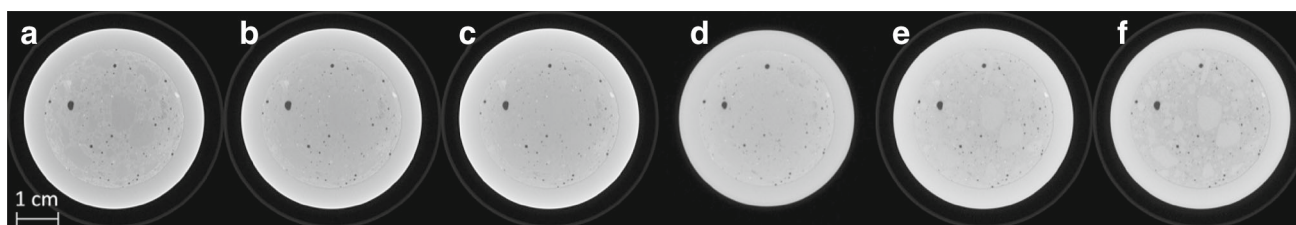


Fig. 2 CT images of a concrete specimen with different X-ray tube and filter settings. From left to right: **a** 100 kV, 1 mm Al filter; **b** 150 kV, 1 mm Al filter; **c** 200 kV, 1 mm Al filter; **d** 250 kV, 0.5 mm Cu filter;

e 280 kV, 1 mm Al+0.25 mm Cu filter; **f** 300 kV, 1 mm Cu filter. The corresponding signal-to-noise ratio of these CT images was 25.8, 27.6, 26.7, 42.0, 25.5 and 24.1, respectively

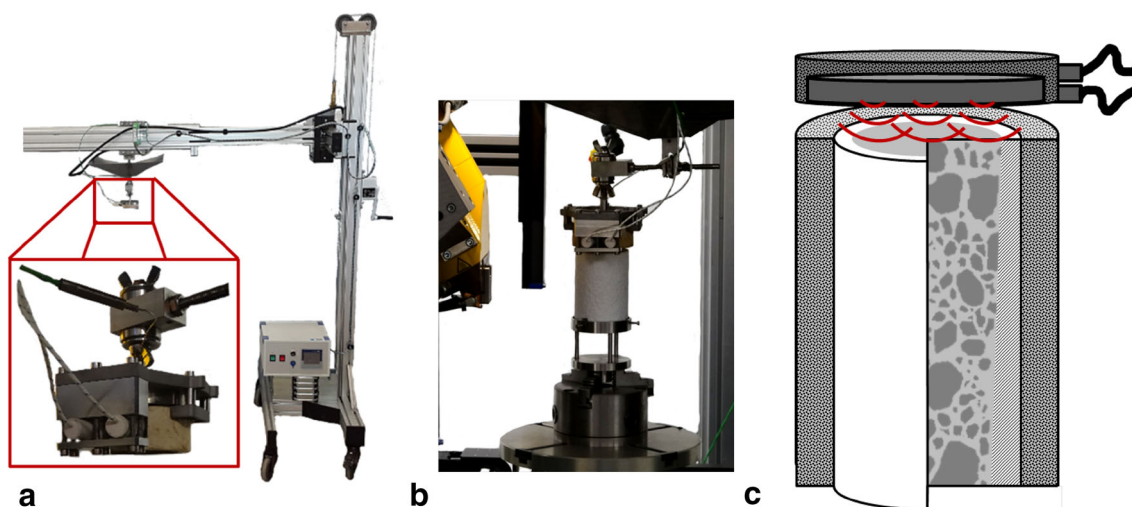


Fig. 3 Heating device (**a**); the in-situ CT test configuration, including the specimen and the heating device (**b**) and schematic depiction of the thermal loading setup (**c**)

tioned 16 mm above the sample surface and irradiated heat to the sample surface across the small air-gap. This radiation-based heating method was used to enable free rotation of the specimen during the CT scanning, in spite of the fixed position of the heating device. Using this combined heating and positioning device, it was possible to generate a repeatable heating regime on the surface of the specimen.

In order to simulate the conditions during explosive spalling, which occurs during the first minutes of a fire at concrete temperatures between 250 and 400 °C [28], a maximum temperature of the heated concrete surface of 300 °C was chosen. This temperature was reached within 28 min of the start of the experiment with a heating rate of approximately 10 K/min. After the maximum surface temperature of the specimen was reached, this temperature was held constant for 130 min.

Unfortunately, it was not possible to measure the actual temperature of the specimen during the heating procedure because any embedded temperature sensor (for example a thermocouple of type K) would cause artefacts in the X-ray projection images. Therefore, the heating regime was validated in a separate set of (off-line) experiments using

specimens with embedded thermocouples. In these experiments, the temperature on the specimen surface was recorded throughout the heating routine. Afterwards, the recorded temperature profile was used to control the heating of the specimen during the actual heating experiment with simultaneous X-ray CT.

During the X-ray CT experiment, after the collection of an initial image of the unheated specimen, the heating device was activated. After 10 min, a series of 10 further scans were completed in 15 min time increments. The acquisition period for each scan was approximately 10 min long. Thus, the average time of applied heating during each scan was 0, 15, 30, 45, 60, 75, 90, 105, 120, 135 and 150 min, respectively.

Given that the moisture conditions in the sample continued to change throughout the 10 min scanning period, the moisture measured in each resulting image represents an average of moisture conditions over the scanning period. Blurring in the resulting images due to this 10 min acquisition process was most severe during the initial scans, when the moisture front was moving the fastest and less significant as the moisture front began to slow during the later stages of heating. Overall, however, despite this averaging effect, it was still

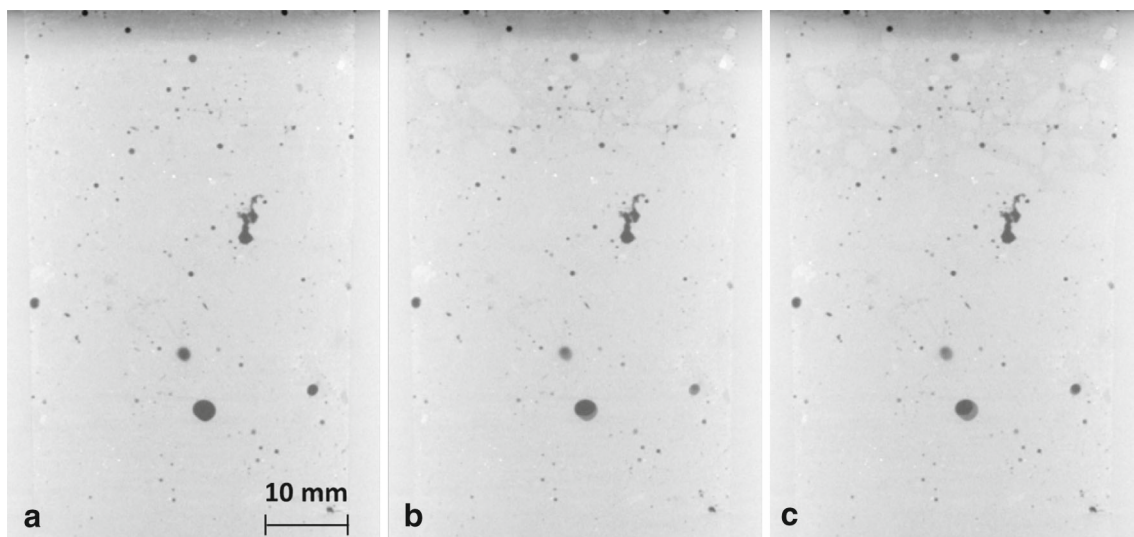


Fig. 4 Vertical slice of the density of the specimen after **a** 0 (reference), **b** 75, and **c** 150 min of heating

possible to obtain high-quality images of moisture conditions in the sample, even during initial heating stages.

3 Image Processing

3.1 Subtraction-Based Image Evaluation

In order to reconstruct 3D-CT images from the 2D X-ray projections, the standard FDK algorithm was used [29]. Prior to this reconstruction, the images had been corrected for beam-hardening effects using a BAM-developed algorithm based on [30]. This beam-hardening correction was essential in order to accurately identify the pores within the high-strength concrete during later analysis steps.

In order to evaluate changes in the moisture distribution within the specimen, fluctuations in the brightness of voxels (3D pixels) in the CT images corresponding to density variations were measured. This was completed through an image subtraction process [31]. The change of the local density, ρ , of the specimen at some point x in space for states i, j corresponding to time-points $t_i < t_j$ is:

$$\Delta\rho_{i,j}(x) := \rho_j(x) - \rho_i(x) \quad (1)$$

In this investigation, the image of the unheated specimen corresponded to time point t_i . Subsequent images of the heated specimen were substituted for the image corresponding to t_j in order to measure temporal variation in moisture distribution (Fig. 4). Within these greyscale images, the brightness of the mortar matrix corresponds to approximately 145 grey-values, the brightness of the internal pores corresponds to approximate 35 grey-values and the brightness of the water condensation corresponds to approximately

75 grey-values. All grey-values are stated in terms of 8-bit intensity.

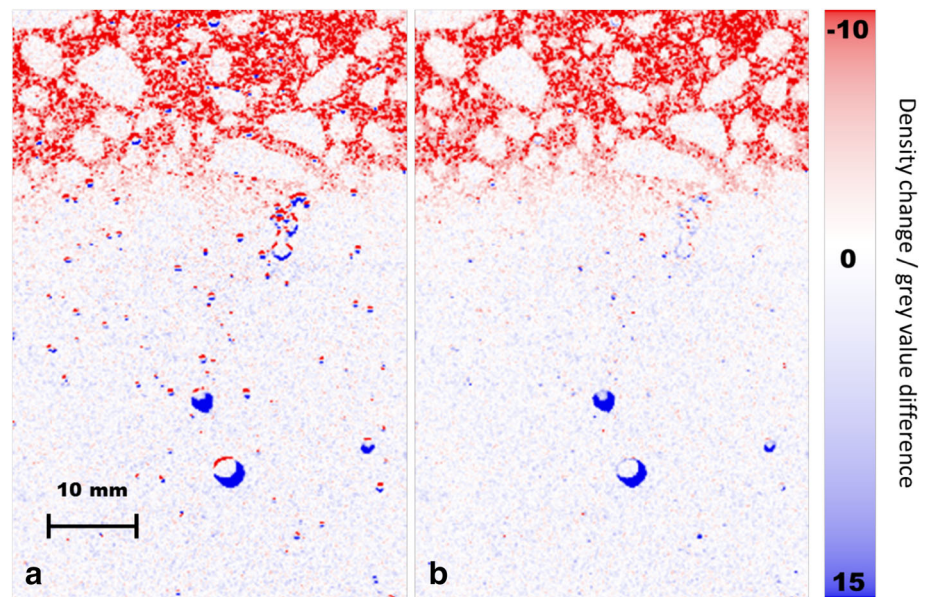
The relationship in Eq. 1 is valid as long as there is no shift between the states i, j . Unfortunately, this condition is, in general, not fulfilled because of significant local geometric shifts, $\Delta_i(x)$, within the specimen. These shifts are due to both thermal expansion and drying-related shrinkage of concrete. These geometric variations lead to density change artefacts in the resulting subtraction images, which are caused by geometrically mismatched specimen regions with significantly different density (Fig. 5). The differences resulting from moisture change range from -15 to $+40$ grey-values (8-bit), which amounts to approximately -10% and $+28\%$ of the mortar matrix grey-values in the original images, respectively. The shift-artefacts, in contrast, lead to differences as high as 100 grey-values along the edges of pores.

3.2 Digital Volume Correlation (DVC)

Far more accurate results can be obtained through the use of greyscale images with corrected spatial coordinates, $\tilde{x}_i(x) = x + \Delta_i(x)$, in Eq. 1. Such a correction can be successfully carried out using DVC-based methods, which are a set of 3D image processing techniques, whereby localized displacement fields are calculated between two images of the same specimen. First developed only for two-dimensional (2D) analysis, DVC has been extended over the last two decades to enable analysis of 3D-CT images [32], due to the rapid progress of computer technology.

Although DVC algorithms have been reported with an accuracy of better than 1% of voxel size [33, 34], the actual DVC results are strongly dependent on the quality of individual images and are significantly affected by the size of

Fig. 5 Difference images without (a) and with DVC-correction (b). These difference images resulted from subtracting the CT images at reference state 0 from those after 150 min heating. The density change scale is in units of 8-bit image intensity. The significant shift artefacts on the pores edges and the prominent improvement due to the DVC-correction are clearly visible



the image subsets selected for comparison, the noise content of the images, and the structure of the material undergoing analysis. It was also hypothesized that variations in the material density (and thus image brightness) of specimen regions in subsequent images could have a negative impact on the performance of DVC algorithms, although no known analysis of this effect has been carried out up to the present time. This was of particular concern for this analysis, since both drying (in the upper regions of the specimen) and moistening (in the lower regions of the specimen) were expected.

Throughout this project, a BAM-developed DVC program written in Python was used in order to align the images. This program uses a 3D-variant of the relatively noise-robust and time-efficient phase-only-correlation method (POC) [35], based on the Fast Fourier Transform (FFT). In order to calculate the image shifts, the images are first divided into sub-volumes of $32 \times 32 \times 32$ voxels in size. The matching pairs of image-subsets, φ , ψ , are then transformed into Fourier space, yielding $\tilde{\varphi}$, $\tilde{\psi}$. The complex product $\tilde{\varphi}^* \times \tilde{\psi}$ is then normalized point-by-point and the Inverse Fourier Transform of the output is calculated. This results in the phase-only correlation function. The peak location of this function represents the relative shift between the two corresponding sub-volumes. An estimate of the relative subset-shifts with sub-pixel resolution is then obtained by means of the sinc-function approximation [35]. Finally, the calculated shift-values are linearly interpolated for every point of the image, and the grey-value corresponding to the calculated voxel-shift is computed, yielding images that are sub-volume-wise registered to the reference image.

The accuracy of the calculated shift-values resulting from this BAM-developed DVC algorithm has been estimated to be approximately 10% of the voxel size in a separate study (publication in preparation) and the mean calculation time needed for DVC registration of a single CT image from these experiments was approximately 150 s on a single computing core of an Intel(R) Xeon(R) CPU E5-2690 v2 running at 3.00 GHz. Subtraction images after DVC-registration using this algorithm showed a significant reduction in deformation-related artefacts (Fig. 5).

4 Experimental Results and Discussion

4.1 Qualitative Moisture Analysis

The sequential CT images (Fig. 4) exhibited progressive decreases in density within the upper 20% of the specimen. This effect is even more clearly visible within the subtraction images (Fig. 6). The front of the diminishing density values parallel to the top of the image is systematically moving downwards reaching the depth of about 20 mm after 150 min. This phenomenon can be interpreted as the expected drying of the top of the specimen due to heating. In the lower portion of the specimen images, pore regions with positive density changes can be observed. This provides an indication that steam from the top of the specimen travels away from the heated surface and condenses in the pores located further from the heat source. This steam condensation occurs as a result of the decreased temperature and pressure levels within these pores.

A closer look at the pores volumes (Fig. 7) shows the time- and space-dependency of the phenomena. It can be observed

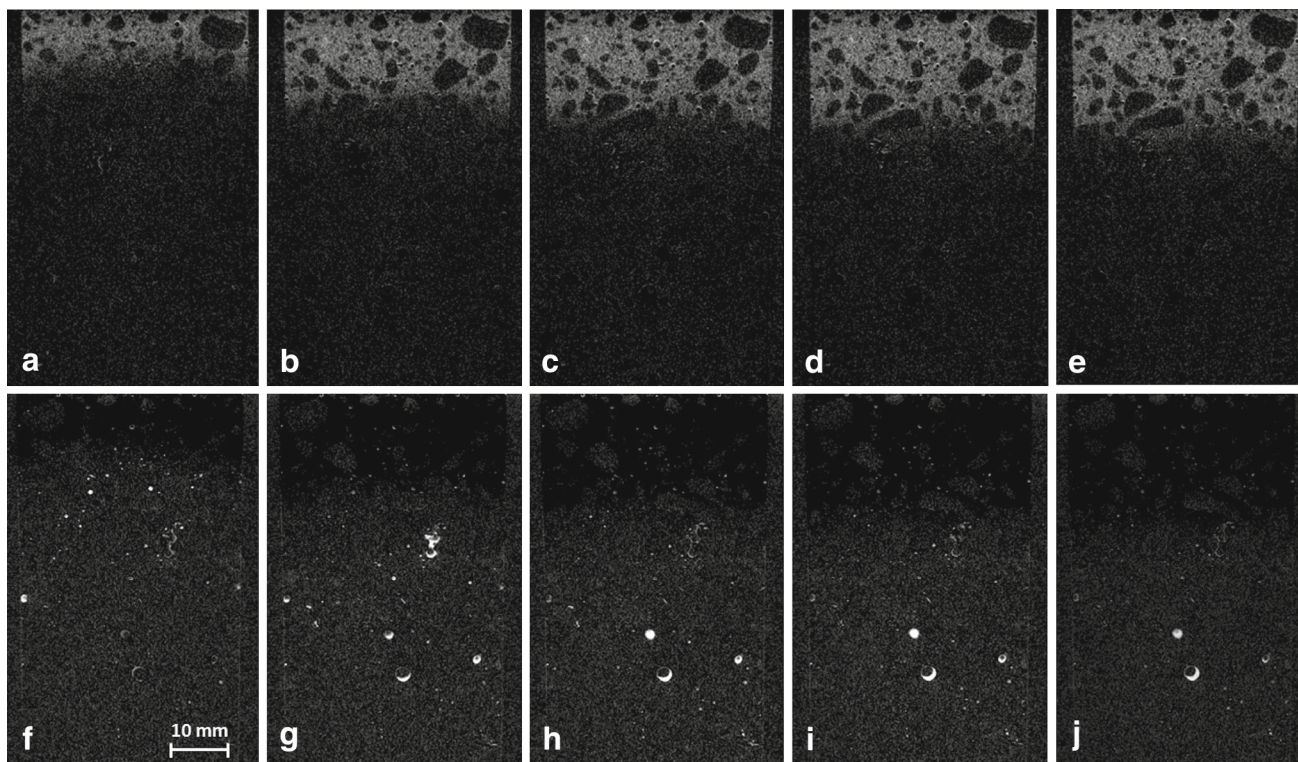
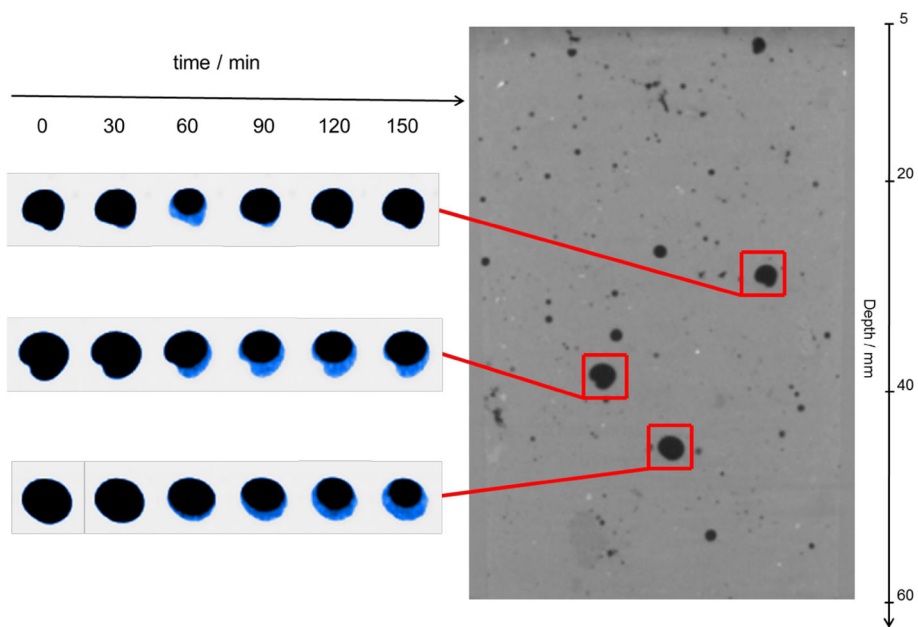


Fig. 6 Image differences calculated at time increments of 30 min relative to the reference measurement (time 0). The negative subtraction part (i.e. drying) is visible in the upper row (a–e) and the positive sub-

traction part (i.e. moistening) is visible in the lower row (f–j). Water condensation in the pores is clearly visible in the later images

Fig. 7 Density changes in selected pores during incremental heating up to 150 min. The blue colour palette was used for clarity (Color figure online)



that water condensation in pores located 20 to 30 mm from the specimen surface begins to disappear after approximately 60 min of heating. The condensation within pores in the lowest regions of the specimen, however, continues to grow up to 150 min.

4.2 Quantitative Moisture Analysis

The performance of the detector system was found to change significantly during the course of the experiments. It is thought that these variations were primarily due to image

burn-in and X-ray scattering due to changing water conditions in the specimen. Although these errors were small compared to overall greyscale image range, they had a significant impact on the quantitative analysis of the subtraction images, which requires much higher levels of greyscale precision.

To correct for these errors, a procedure was implemented, in which materials that were considered to possess constant density were used as calibration points. In this procedure, the high-density ceramic and low-density aluminium silicate wool materials were used to define the bright and dark calibration points in each image, respectively. Filters were then created that ensured that the respective average brightness of ceramic and aluminium silicate wool in each slice remained constant throughout all the images. By using these two reference points and linearly interpolating the filter parameters for all intermediate greyscale values, the errors introduced by variations in detector performance could be significantly mitigated.

In order to quantify the results of the experiments, changes in voxel greyscale were converted into moisture percentage estimates. This was completed by recording the greyscale difference in pores that went from an unsaturated to a fully saturated state during the experiments. This greyscale difference was taken to represent 100% change in moisture and regions with no greyscale change between scans were considered to represent 0% change in moisture. Thus, by using these two reference points and linearly interpolating between them, all other greyscale values could be converted to corresponding moisture-change values.

After correction for variations in detector performance, and conversion of greyscale values to moisture percentages, images representing moisture transport in the concrete specimen could be depicted (Fig. 8). A 3D-rendered depiction of the distribution of the moisture changes is shown in Fig. 9. It was also possible to calculate the average moisture change relative to specimen height for both the entire specimen cross-section and for the sole portion of the cross-section filled with matrix and aggregates, i.e. excluding the pores (Fig. 10). For the analysis of matrix and aggregates, the regions of the image corresponding to the dilated pores were removed prior to calculation of the moisture plots. This pore dilation was necessary to ensure that the regions along the edge of the pores were fully removed, since they could introduce significant additional errors. It is thought that the moisture changes measured in upper-most and lower-most regions of the images are primarily due to cone-beam artefacts in the CT-images rather than actual material behaviour. For this reason, the data from the top 5 mm of the specimen have been removed from the Figs. 7, 8, 9, and 10.

The quantitative data from this analysis indicates the presence of significant drying within a progressively growing upper-region of the sample. As the heating time increases, it can also be observed that the increase in drying depth deceler-

ates. Given that the content of chemically unbound moisture within concrete matrix material is generally considered to remain around 11% by volume. These results indicate that chemically-bound water was also released within the drying regions of the specimen during the heating.

Positive moisture changes are also visible both within the plot for all sample material and within the plot for only matrix and aggregate. This provides an indication that although moisture increase can only be qualitatively observed within the pores, moisture increase within the matrix and aggregate is also present. This ability to differentiate between moisture transport in different material types is a clear advantage offered by quantitative CT analysis over most other conventional non-destructive moisture analysis methods.

4.3 Evaluation of the DVC Technique

Through qualitative comparison of the uncorrected and DVC-corrected subtraction images alone, it is clear that the DVC technique significantly diminishes shift-related image differences (Fig. 5). However, some significant shift artefacts can still be observed at the edges of the pores, where there is a substantial grey value change of up to 100 grey value levels. To estimate this error in the shift field, the edge of a large pore in the centre of the volume, which was not influenced by the moisture changes, was selected. Due to the given boundary conditions, the maximum error of the DVC correction was calculated to be approximately 0.2 voxels.

In order to demonstrate the impact of the DVC correction, the absolute values of grey value differences (the residuals) averaged over each slice within the subtraction images were evaluated (Fig. 11a). These residuals, which are minimized during the DVC alignment procedure, contain actual image changes (like moisture changes) as well as shift artifacts and noise. The noise level in the original CT images amounts to about 2 grey values on this scale, which can be seen in Fig. 11a in the lower part of the sample (depth above 50 mm), where there are only small physical changes. The larger mean value of residuals in the top part (depth below 20 mm) are caused by the drying effect discussed earlier, and even residual increases, due to water condensation in the pores, can be seen at a depth of 30 mm and 40 mm. Comparisons of the residual values for the corrected and uncorrected images show that the corrected value can be as much as 20% lower than uncorrected one (Fig. 11b). It can, therefore, be concluded that the application of the DVC image correction leads to an improvement of the accuracy of up to 20%.

5 Conclusions and Outlook

In this investigation, a standard laboratory CT system was successfully used for in situ detection of heat-induced mois-

Fig. 8 Depiction of moisture transport after increments of 30, 60, 90, 120 and 150 min, respectively (Color figure online)

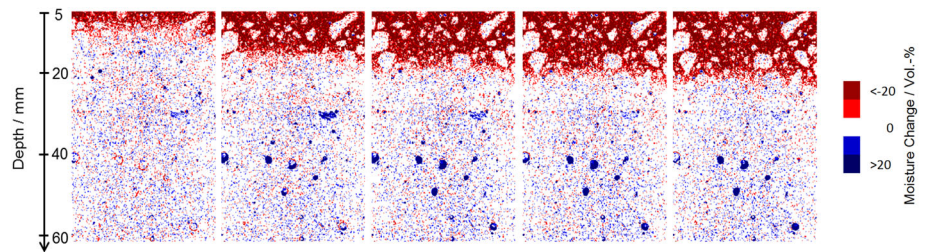


Fig. 9 3D-rendered density changes after **a** 30, **b** 60 and **c** 90 min. Red—negative changes (drying of the cement matrix) and blue—positive (moisture accumulation in pores) (Color figure online)

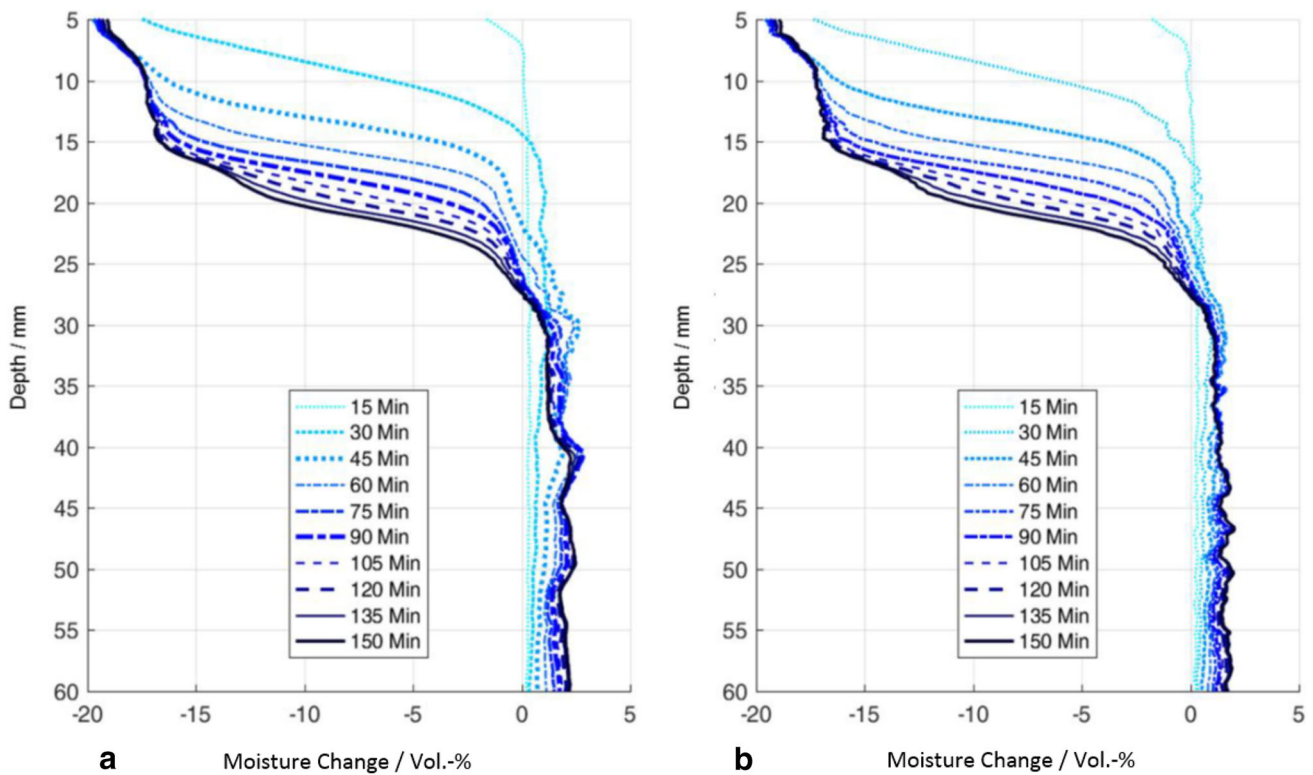
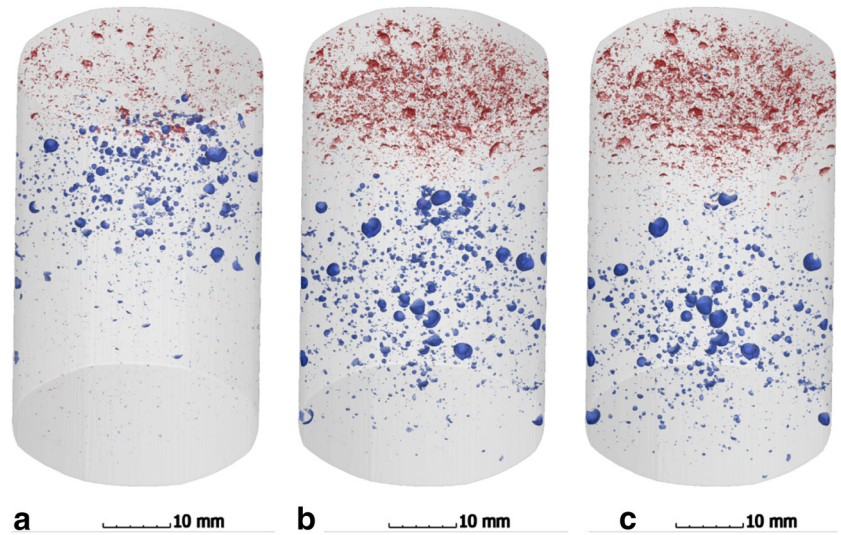


Fig. 10 Plot of average moisture change relative to specimen height for all specimen material (a) and for only matrix and aggregate (b)

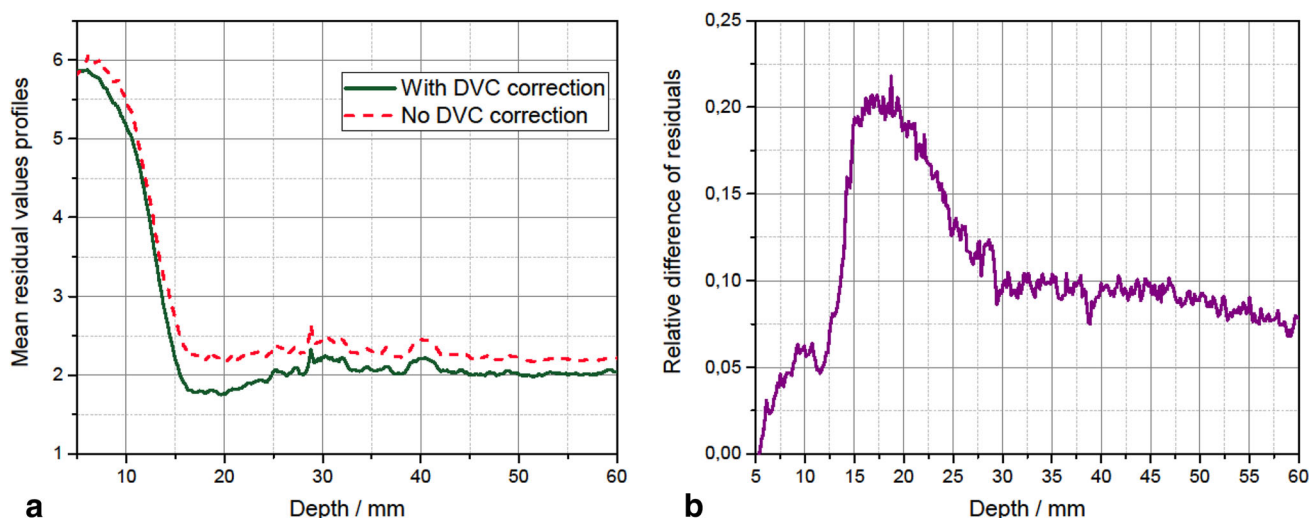


Fig. 11 Profiles of mean residuals for uncorrected and DVC-corrected images (a) calculated for 45 min of heating relative to the image of the unheated sample. The relative differences (b) between the uncorrected

and DVC-corrected images exhibit a residual reduction of up to approximately 20%, which corresponds with a reduction in shift artefacts

ture changes in concrete. The results of these experiments clearly demonstrate that this widely-available measurement system is capable of rapid density change evaluation in concrete and other building materials. Other research applications, where a similar experimental approach could prove to be useful include water transport due to capillary action in porous materials, the progression of curing of cast materials such as concrete and movement of moisture within organic structures such as plant stems.

The results of this research program demonstrated the tendency of moisture within heated areas of the concrete matrix to evaporate, travel away from the specimen surface and re-condense in cooler, lower pressure regions deeper within the sample, and most notably, in the pores. It was also shown, however, that in addition to pore condensation, moisture increase in the concrete matrix itself can be measured using quantitative analysis methods (after corrections for variations in detector performance). This ability to differentiate between moisture transport processes in different component materials of the specimen is a clear advantage of the CT-based procedure over other common non-destructive testing techniques. Even though the measurement time was reduced to 10 min for one full 3D scan, there is still significant change in the sample over this time span. For further investigations, faster data acquisition could be useful.

It was further demonstrated that the use of DVC can significantly reduce measurement error during expansive test conditions. The accuracy of subtraction-based image analysis methods is particularly sensitive to such deformation-related errors. It is also clear, however, that significant improvements in the accuracy of current DVC image analysis tools is needed. For such improvements, it will be important to

develop a general framework for assessing the relative validity and accuracy of various DVC techniques.

The results of the analysis of the thermally-induced moisture transport in high-strength concrete contribute to the development of deeper insights into the thermo-hydral processes in thermally-exposed concrete. Using the developed methodology, consisting of a suitable specimen with a double-layer casing, an adapted X-ray CT measurement regime, and reconstruction and image processing algorithms, different influencing parameters on the spalling behavior of concrete can be investigated. As an example, the influence of adding polypropylene fibers (PP-fibers) to the concrete recipe on the thermally-induced moisture transport should be mentioned. The addition of PP-fibers is a recognized method for avoiding explosive spalling [36]. The PP-fibers induce micro-cracks and connect these. As a result of fiber melting, an extensive crack network is created. This leads to a significant increase of the permeability and a reduction of the pore pressure build-up. The analysis of fiber influence on the moisture transport is the subject of ongoing investigations using the methodology presented in this paper.

Acknowledgements The authors would like to acknowledge their gratitude to Dr. Illerhaus, Mr. Meinel and Mr. Onel for their support and advice regarding CT scanning techniques and analysis methods. The work was internally funded by the Bundesanstalt für Materialforschung und -prüfung (BAM) through the Menschen-Ideen-Strukturen (MIS) Program.

References

1. Kordina, K.: Planung unterirdischer Verkehrsanlagen gegen Brandgefahren. In: Tunnel (2004)

2. Kalifa, P., Chéné, G., Gallé, C.: High-temperature behaviour of HPC with polypropylene fibres From spalling to microstructure. *Cem. Concr. Res.* **31**, 1487–1499 (2001)
3. Jansson, R., Boström, L.: Fire spalling—the moisture effect. In: Dehn F., Koenders, E.A.B. (eds.) 1st International Workshop on Concrete Spalling due to Fire Exposure, Leipzig. pp. 120–129 (2009)
4. Van der Heijden, G.H.A., et al.: One-dimensional scanning of moisture in heated porous building materials with NMR. *J. Magn. Reson.* **208**, 235–242 (2011)
5. Weber, B., et al.: Neutron radiography of heated high-performance mortar. *MATEC Web Conf.* **6**, 8 (2013)
6. Toropovs, N., et al.: Real-time measurement of temperature, pressure and moisture profiles in high-performance concrete exposed to high temperatures during neutron radiography imaging. *Cem. Concr. Res.* **68**, 166–173 (2015)
7. Powierza, B.: In-Situ CT observation of water migration in heated concrete. In: 3rd International Conference on Tomography of Materials and Structures, Lund, Sweden (2017)
8. Stelzner, L., et al.: Analysis of moisture transport in unilateral-heated dense high-strength concrete. In: 5th International Workshop on Concrete Spalling due to Fire Exposure, Borås, Sweden (2017)
9. Masschaele, B., et al.: High-speed thermal neutron tomography for the visualization of water repellents, consolidants and water uptake in sand and lime stones. *Radiat. Phys. Chem.* **71**(3–4), 807–808 (2004)
10. Hillenbach, A., et al.: High flux neutron imaging for high-speed radiography, dynamic tomography and strongly absorbing materials. *Nucl. Instrum. Methods Phys. Res. Sect. A* **542**(1–3), 116–122 (2005)
11. Martz, H.E., et al.: Computerized-tomography analysis of reinforced-concrete. *ACI Mater. J.* **90**(3), 259–264 (1993)
12. Morgan, I.L., et al.: Examination of concrete by computerized-tomography. *J. Am. Concr. Inst.* **77**(1), 23–27 (1980)
13. Flannery, B.P., et al.: Three-dimensional X-ray microtomography. *Science* **237**(4821), 1439–1444 (1987)
14. Feldkamp, L.A., Davis, L.C., Kress, J.W.: Practical cone-beam algorithm. *J. Opt. Soc. Am. A* **1**(6), 612–619 (1984)
15. Landis, E.N., Nagy, E.N., Keane, D.T.: Microtomographic measurements of internal damage in portland-cement-based composites. *J. Aerosp. Eng.* **10**(1), 2–6 (1997)
16. Asahina, D., Landis, E.N., Bolander, J.E.: Modeling of phase interfaces during pre-critical crack growth in concrete. *Cem. Concr. Compos.* **33**(9), 966–977 (2011)
17. Poinard, C., et al.: Compression triaxial behavior of concrete: the role of the mesostructure by analysis of X-ray tomographic images. *Eur. J. Environ. Civ. Eng.* **16**, S115–S136 (2012)
18. Oesch, T.S., Landis, E.N., Kuchma, D.A.: Conventional concrete and UHPC performance-damage relationships identified using computed tomography. *J. Eng. Mech.* **142**(12), 531–538 (2016)
19. Oesch, T.S.: In-Situ CT investigation of pull-out failure for reinforcing bars embedded in conventional and high-performance concretes. In: 6th Conference on Industrial Computed Tomography (ICT), Wels, Austria: NDT.net (2016)
20. Paetsch, O., et al.: 3D corrosion detection in time-dependent CT images of concrete. In: Digital Industrial Radiology and Computed Tomography Conference, Ghent, Belgium (2015)
21. Yang, L., et al.: In-Situ tracking of water transport in cement paste using X-ray computed tomography combined with CsCl enhancing. *Mater. Lett.* **160**, 381–383 (2015)
22. Boone, M.A., et al.: 3D mapping of water in oolitic limestone at atmospheric and vacuum saturation using X-ray micro-CT differential imaging. *Mater. Charact.* **97**, 150–160 (2014)
23. Yang, F., et al.: Visualization of water drying in porous materials by X-ray phase contrast imaging. *J. Microsc.* **261**(1), 88–104 (2016)
24. Wildenschild, D., et al.: Using X-ray computed tomography in hydrology: systems, resolutions, and limitations. *J. Hydrol.* **267**(3), 285–297 (2002)
25. Wildenschild, D., et al.: Quantitative analysis of flow processes in a sand using synchrotron-based X-ray microtomography. *Vadose Zone J.* **4**(1), 112–126 (2005)
26. Dauti, D., et al.: Analysis of moisture migration in concrete at high temperature through in situ neutron tomography. *Cem. Concr. Res.* **111**, 41–55 (2018)
27. Schneider, U.: Compressive strength for service and accident conditions. *Mater. Struct.* **28**(181), 410–414 (1995)
28. Kalifa, P., Menneteau, F.-D., Quenard, D.: Spalling and pore pressure in HPC at high temperatures. Papers presented at the symposium on transport properties and microstructure of cement-based systems, vol. 30, pp. 1915–1927 (2000)
29. Feldkamp, L.A., Davis, L.C., Kress, J.W.: Practical cone-beam algorithm. *J. Opt. Soc. Am. A* **1**(6), 612–619 (1984)
30. Rüeeggger, P., et al.: Standardization of computed tomography images by means of a material-selective beam hardening correction. *J. Comput. Assist. Tomogr.* **2**(2), 184–188 (1978)
31. Weise, F., Onel, Y., Goebbels, J.: Analyse des Gefüge- und Feuchtezustandes in mineralischen Baustoffen mit der Röntgen-3D-Computertomografie. *Bauphysik* **29**(3), 194–201 (2007)
32. Bay, B.K., et al.: Digital volume correlation: three-dimensional strain mapping using X-ray tomography. *Exp. Mech.* **39**(3), 217–226 (1999)
33. Roberts, B.C., Perilli, E., Reynolds, K.J.: Application of the digital volume correlation technique for the measurement of displacement and strain fields in bone: a literature review. *J. Biomech.* **47**(5), 923–934 (2014)
34. Alba, A., et al.: Phase correlation with sub-pixel accuracy: a comparative study in 1D and 2D. *Comput. Vis. Image Underst.* **137**(Suppl C), 76–87 (2015)
35. Foroosh, H., Zerubia, J.B., Berthod, M.: Extension of phase correlation to subpixel registration. *Trans. Image Proc.* **11**(3), 188–200 (2002)
36. DIN, V., 1-2 Eurocode 2: Planung von Stahlbeton-und Spann-betontragwerken-Teil 1-2: Allgemeine Regeln-Tragwerksbemessung für den Brandfall, Ausgabe Dezember (2010)